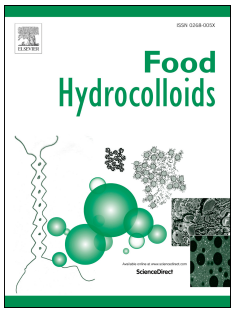

Lactoferrin as a carrier of iron: Development and physicochemical characterization

Arlete M. Marques, Ana I. Bourbon, Rui M. Rodrigues, José A. Teixeira, Lorenzo M. Pastrana, Miguel A. Cerqueira

PII: S0268-005X(23)00318-1

DOI: https://doi.org/10.1016/j.foodhyd.2023.108772

Reference: FOOHYD 108772

To appear in: *Food Hydrocolloids*

Received Date: 29 September 2022

Revised Date: 25 March 2023

Accepted Date: 12 April 2023

Please cite this article as: Marques, A.M., Bourbon, A.I., Rodrigues, R.M., Teixeira, José.A., Pastrana, L.M., Cerqueira, M.A., Lactoferrin as a carrier of iron: Development and physicochemical characterization, *Food Hydrocolloids* (2023), doi: https://doi.org/10.1016/j.foodhyd.2023.108772.

Credit authorship contribution statement

Conceptualization, A.M.M., A.I.B., R.M.R., J.A.T., L.M.P., M.A.C.; Methodology, A.M.M., A.I.B., R.M.R., J.A.T., L.M.P., M.A.C.; Investigation, A.M.M., A.I.B., R.M.R., J.A.T., L.M.P., M.A.C.; Formal analysis, A.M.M.; Writing-original draft preparation, A.M.M.; Writing-review and editing, A.M.M., A.I.B., R.M.R., J.A.T., L.M.P., M.A.C.; Supervision, A.I.B., R.M.R., J.A.T., L.M.P., M.A.C.; All the authors have read and agreed to the published version of the manuscript.

Bovine Lactoferrin protein

$FeSO_4$ (Fe^{2+})

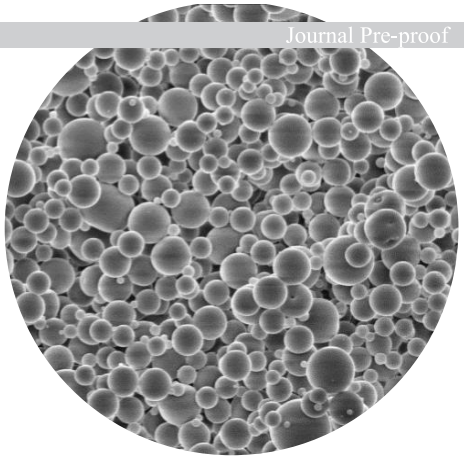

Lactoferrin-Fe Micro and nano particles

- Circular Dichroism
- Fluorescence
- Native polyacrylamide gel electrophoresis
- Thermogravimetric analyses
- Attenuated total reflectance Fourier transform infrared spectroscopy
- Iron release test at pH=2 and pH=7

Nano Spray Dryer B-90 HP

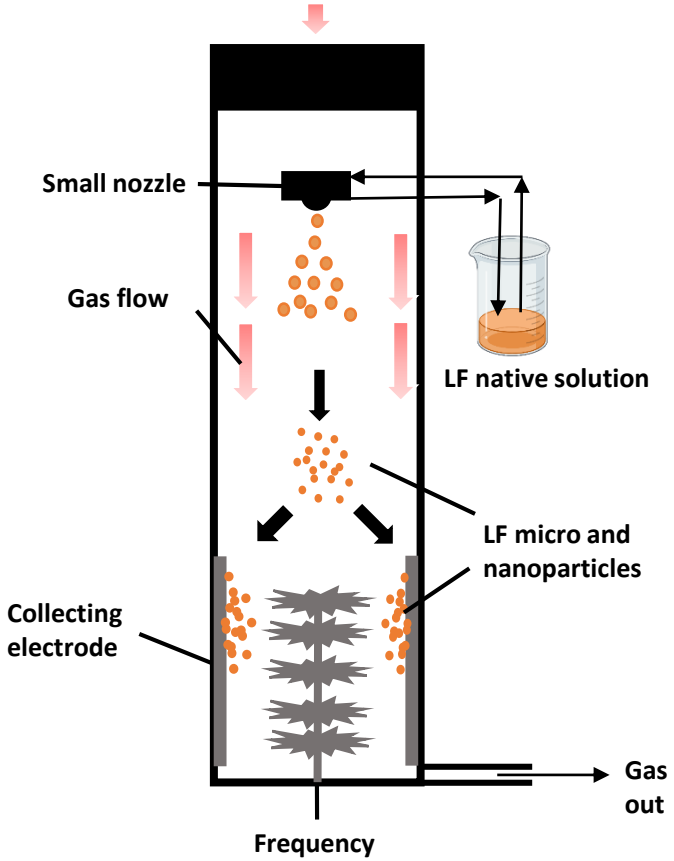

Lactoferrin as a carrier of iron: development and physicochemical characterization

Arlete M. Marques[1,2,3,*], Ana I. Bourbon[2], Rui M. Rodrigues[1,3], José A. Teixeira[1,3], Lorenzo M. Pastrana[2], Miguel A. Cerqueira[2]

1- Centre of Biological Engineering, University of Minho, Campus de Gualtar, 4710-057, Braga Portugal

2- International Iberian Nanotechnology Laboratory, Av. Mestre José Veiga, 4715-330, Braga, Portugal

3- LABBELS – Associate Laboratory, Braga/Guimarães, Portugal

*Corresponding author: arlete.marques93@gmail.com

Abstract

Iron deficiency is the main cause of anemia, one of the most common nutritional deficiencies affecting millions of people worldwide. In addition, iron instability, sensitivity, and intense flavor limit its use in food fortification. In this work, lactoferrin (LF) particles were developed by Nano Spray Dryer (NSD) and its capacity to be used as an iron carrier was evaluated. The effect of NSD temperature (60 °C, 80 °C, and 100 °C) and LF concentrations (10 mg.mL^{-1}, 50 mg.mL^{-1}, and 100 mg.mL^{-1}) was evaluated on the LF structure and on the production and stability of a LF-iron carrier. Results showed that the NSD is suitable for producing LF particles with diameters ranged from 38.8 nm to 4533.6 nm. Although different surface morphologies were obtained, higher protein concentrations (100 mg.mL^{-1}) produced round shape and smooth surface particles, but for lower protein concentrations (10 mg.mL^{-1} and 50 mg.mL^{-1}) wrinkled particles and doughnut shape particles were obtained. SDS-page electrophoresis and circular dichroism (CD) for secondary structure (185 – 260 nm) show that the characteristics of the structures were maintained, meaning that NSD does not cause protein degradation. CD for tertiary structure (250 nm – 350 nm) and fluorescence tests confirmed the interaction between LF and iron, observed by an intensity decrease and a wavelength shift in fluorescence spectra. The CD tertiary structure analysis showed higher ellipticity for the Trp peak, meaning conformational changes in the neighbor amino acids due to protein-iron interaction. Iron release experiments were performed at different pH values (2.0 and 7.4) at 37 °C aiming to understand the release mechanism in different media. Results showed that at pH 2 the iron release could be described by the linear superposition model ($Radj^2$=0.9879) (explained by Fick and relaxation phenomenon) and that at pH 7.4 there is no iron release, showing that particles are stable at neutral pH. NSD is a suitable technology for producing iron-loaded protein-based carriers that could be used in food applications.

Keywords: Food fortification; iron deficiency anemia; milk protein; health; Nano Spray Dryer.

1. Introduction

It is estimated that anemia, mostly caused by iron deficiency, affects 33% of non-pregnant women, 40% of pregnant women, and 42% of children worldwide (World Health Organization, 2020). Iron is a micromineral that helps metalloproteins like myoglobin, hemoglobin, and oxidases in reduction and oxidation reactions (Fathima et al., 2017). The lack of iron in humans results on fatigue symptoms, low physical performance, poor growth and brain development, and a weak immune system (Lozoff, 2007; Marques et al., 2019; Menza & Probart, 2013). Iron deficiency can have different causes, such as an inadequate intake due to diets poor in iron, by blood loss, or even poor iron absorption because of intestinal conditions or interaction with other compounds that prevent absorption (e.g., dairy products) (Marques et al., 2019; Percy et al., 2017; World Health Organization, 2020).

Aiming to increase the ingestion of iron and meet the daily recommended intake together with avoiding health problems related to malnutrition, strategies such as diversification of diets, iron supplementation, and even food fortification were proposed (Marques et al., 2019; Shubham et al., 2020). However, direct iron addition to food has some drawbacks that mainly result in iron instability and intense flavor, limiting its use in food products (Fathima et al., 2017; Katouzian & Jafari, 2016; Marques et al., 2019; Shubham et al., 2020). One of the ways to preserve and maintain the properties of micronutrients and improve their functionality and bioavailability is their encapsulation. The encapsulation using natural carriers is a way to protect the micronutrients from adverse factors, promote a controlled release, and mask undesirable flavors, which increases their application in food products (Gharibzahedi & Jafari, 2017; Marques et al., 2019). Some works encapsulated the mineral iron using different materials and encapsulation techniques. Hatefi and Farhadian (2020) encapsulated iron (ferrous sulphate) in solid lipid nanoparticles with a size of 358 ± 21.9 nm, while Gupta et al. (2015) used a blend of gum arabic, maltodextrin, and modified starch for the iron encapsulation using the solvent evaporation method. An iron delivery system was developed by Katuwavila et al. (2016) using controlled ionic gelation to produce alginate particles with a size range from 15 nm to 30 nm and loaded with ferrous sulphate. Churio and Valenzuela (2018) produced maltodextrin particles to encapsulate heme (bovine erythrocytes) and non-heme (ferrous sulphate) iron, and in another work developed by Wardhani et al. (2020), hydrolyzed glucomannan was used for the ferrous sulphate encapsulation. Both works used spray drying technology to produce the particles. Micro- and nanoscale carriers have advantages, like good stability against aggregation and sedimentation, enhanced solubility, controllable release and diffusion rates, and increased absorption in the gastrointestinal (GI) tract (Marques et al., 2019; Martins et al., 2016). Previous work has also shown that protein-based micro and

nanocarriers can be an interesting technique for protecting micronutrients like iron (Martins et al., 2016).

Bovine lactoferrin (LF) is a protein from the transferrin family and consists of a single polypeptide chain with a molecular weight of around 78 kDa with 703 amino acids and an isoelectric point around 8-9 (Bourbon et al., 2015; Levay & Viljoen, 1995; Martins et al., 2016; Wang et al., 2019). LF is a globular protein that has two lobes, C-lobe and N-lobe, and each C- and N-lobe can be divided into two sub-lobes: C1 and C2; N1 and N2. Each lobe can bind an iron ion in a reversible way (Baker & Baker, 2004; Bokkhim et al., 2014; Wang et al., 2019). In terms of iron saturation, there are three different forms of lactoferrin, the native lactoferrin (Native-LF) that is only partially iron-saturated, the iron-free lactoferrin that is called apo-lactoferrin (Apo-LF), and the iron-saturated lactoferrin, called holo-lactoferrin (Holo-LF) (Bokkhim et al., 2014; Wang et al., 2017b, 2019). Lactoferrin presents other functions and functionalities such as antiviral, antibacterial, antifungal, anti-inflammatory, and anticarcinogenic activities. In addition, LF is a natural compound with great biocompatibility, biodegradability, and low toxicity, making it particularly appealing for food applications (Liu et al., 2018).

Some works reported the use of Nano spray drying (NSD) technology to produce bioactive compound-loaded carriers. NSD is a recent technology that dries different types of solutions (aqueous or organic solutions, emulsions, dispersions, and suspensions) to obtain dried particles and encapsulate different bioactive compounds (Arpagaus, 2019b, 2019a; Büchi Labortechnik AG, 2017b, 2017a; Marques et al., 2021).

Oliveira et al. (2013) used Arabic gum, cashew nut gum, sodium alginate, and carboxymethyl cellulose to encapsulate vitamin B12 using NSD technology, while Pérez-Masiá et al. (2015) encapsulated folic acid using whey protein concentrate and resistant starch as wall materials. Other authors used this technology to encapsulate curcumin (Wang et al., 2018; Wang, Ma, et al., 2016; Zhou et al., 2018), vitamins D3 and E, vitamins B3, B6, B12, C and BCAAS (Branched Chain Amino Acids) (Wang, Soyama, et al., 2016), rutin (Pedrozo et al., 2020) and omega-3 fatty acids (Nunes et al., 2020). However, the use of NSD to produce iron-loaded carriers using LF is unexplored. Other works used different technologies to produce iron particles and carriers; for example, thermal gelation (Martins et al., 2016), ionic gelation , high-speed homogenization . (Naveen and Kanum 2014), and melting-lipid-double emulsion (Hatefi and Farhadian 2020).

In the present work, the production of iron-loaded protein-based carriers using NSD, and the effect of the drying process, with and without the addition of iron, on the protein structure, were studied. With that we aim to understand the iron binding capability to the LF during NSD, and the effect of the drying temperature and NSD process on the final properties of LF, and on the iron-loaded carrier. Additionally, the iron release was also evaluated at two different media, acidic and neutral.

2. Materials and methods

Bovine lactoferrin (LF) was purchased from DMV International (USA). LF has a molecular weight (MW) of 83 kDa and an isoelectric point of 8.5. LF composition is expressed as a dry weight percentage of 96% protein, 0.5% ash, 3.5% moisture, and an iron content of around 120 ppm. This purchased commercial LF was dried by spray drying. Iron sulfate ($FeSO_4.xH_2O$) was kindly given by the company Formulab (Maia, Portugal).

2.1 Solution preparation

LF solutions were prepared in a concentration of 10 $mg.mL^{-1}$, 50 $mg.mL^{-1}$ and 100 $mg.mL^{-1}$ using ultra-pure water (milliQ water). Lactoferrin was dispersed by stirring the powder in water at 350 rpm until total dissolution. After that, to avoid NSD blockage and clogging (Büchi Labortechnik AG, 2017a; Harsha et al., 2015; Marques et al., 2021), solutions were centrifuged (Universal 320, Hettick, Germany) at 1780 *g* for 20 minutes to remove any undissolved protein (representing less than 3% of total mass).

For iron addition, different iron quantities were added to the LF solution prepared. Iron sulfate ($FeSO_4.xH_2O$) was added to the LF solution and stirred at 350 rpm in a beaker protected from the light, until total dissolution. Iron quantities were calculated based on: a) the iron amount needed to bind just one binding site, which corresponds to 0.7 mg of iron per gram of LF (NSD80_100_0.7); b) the iron amount needed to bind both binding sites in the LF molecule which corresponds to 1.4 mg of iron per gram of LF (NSD80_100_1.4) (Bokkhim et al., 2014; Sharma, 2019); and c) the iron amount needed to bind both binding sites and has an excess of iron, which corresponds to 2.8 mg of iron per gram of LF (NSD80_100_2.8). The iron sulphate amount was calculated based on the iron content.

2.2 Nano Spray Dryer

Nano Spray Dryer B-90 HP (Büchi, Switzerland) with an open circuit (open loop) was used to dry the different LF solutions (loaded and unloaded). The drying temperatures were selected considering the reported denaturation temperature of LF. It has been reported that native LF has two denaturation temperatures, 60 °C and 90 °C (Bokkhim et al., 2013; Bourbon et al., 2020; Goulding et al., 2021; Wang et al., 2017b, 2019). Therefore, the first temperature considered was 60 °C (NSD60). The second selected drying temperature was 80 °C (NSD80) which is between both denaturation temperatures for LF. The last temperature evaluated was 100 °C (NSD100) which is above both denaturation temperatures.

The other parameters were previously optimized and kept constant for all the solutions: Frequency 120 kHz, the gas flow of 100 mg.mL^{-1}, pump 40%, and the spray 80%. After drying all the solutions, the powder was collected from the cylinder and stored in a desiccator with a relative humidity (RH) of 0%.

2.3 Particles size and morphology

The size and morphology of the obtained powder were evaluated by scanning electron microscopy (SEM) (Quanta 650FEG (FEI Europe B.V., Eindhoven, Netherlands)). The powder was spread onto a carbon tape and then sputtered with gold until achieving a thickness of approximately 10 nm. Samples were examined at 5 kV, spot 3, and a magnification of around 5000x. Particle size distribution was obtained from three different pictures of each sample, measured with Image J 1.52a (Java 1.8.0), and calculated using the software OriginLab - Origin 9 (version 90E) (OriginLab Corporation, Northampton, MA, USA). At least 900 particles were measured for each condition.

2.4 Circular dichroism

Circular dichroism (CD) was used to determine the secondary and tertiary structural changes of the protein after the drying process in the NSD. Obtained powder from NSD was re-hydrated in ultra-pure water and stirred until total dissolution. CD spectra were collected using the CD spectrophotometer Jasco J-1500 (Jasco Inc., Tokyo, Japan). The CD average spectrum of the blank was subtracted from each recorded spectrum. The analyses were performed at room temperature (~22 °C).

For the secondary structure study, the following parameters were used: wavelength ranging from 185 nm to 260 nm, with a scanning speed of 20 nm.min^{-1}; a bandwidth of 1 nm; data pitch of 0.5 nm, a digital integration time (D.I.T) of 1 s and 5 accumulations. Samples with a concentration of 0.1 mg.mL^{-1} were analyzed in a 1 mm path length quartz cell. Samples were studied with a gas flow (N_2) of approximately 10 L.min^{-1}.

In the tertiary structure study, the following parameters were used: a wavelength ranging from 250 nm to 350 nm, on a 10 mm path length quartz cell and solutions with a concentration of 1 mg.mL^{-1}. A scanning speed of 20 nm.min^{-1}, a bandwidth of 1 nm; a data pitch of 0.5 nm, a response D.I.T of 1s and 5 accumulations, and a gas flow (N_2) ranged between 3 to 5 L.min^{-1} was used.

To study changes in the LF structure after the iron addition, 5 mg.mL^{-1} samples were analyzed in the CD equipment with a wavelength ranging between 300 nm to 600 nm. Samples were placed

in a 10 mm path length quartz cell. The following parameters were used during analysis: a scanning rate of 50 $nm.min^{-1}$, 5 accumulations, a response D.I.T of 1s and 5 accumulations. Also, was used a gas flow (N_2) rate of approximately 3 $L.min^{-1}$ to 5 $L.min^{-1}$.

2.5 Native polyacrylamide gel electrophoresis (Native – PAGE)

In order to evaluate NSD temperature effect on the protein structure, Native-PAGE electrophoresis was performed in: LF native samples (LF Nat), LF after drying in NSD (NSD60_10, NSD60_50, NSD60_100; NSD80_10, NSD80_50, NSD80_100; NSD100_10, NSD100_50, and NSD100_100), and also after iron addition (NSD80_100_0.7, NSD80_100_1.4, NSD80_100_2.8). Standard maker Fisher BioReagent EZ-Run Rec Protein Ladder (10–200 kD) (Thermo Fisher Scientific, Massachusetts, EUA) was used to identify the molecular weight of samples.

Native-PAGE electrophoresis was carried out using Mini-Protean Tetra system cell equipped with a PowerPAC Basic power supply (Bio-Rad Laboratories, Hercules, Ca, USA), and 12 wells Mini-Protean TGX precast gels containing 4-15% of polyacrylamide Bio-rad (Bio-Rad Laboratories, Hercules, Ca, USA).

Samples were prepared with a concentration of 2 $mg.mL^{-1}$ and 15 µL was added. Electrophoresis was performed at 20 mA. Then gels were stained using a Comassie Stain Blue solution (Bio-Rad Laboratories, Hercules, Ca, USA).

2.6 Fluorescence determination

Fluorescence determinations were conducted using the fluorescence instrument Aqualog (Horiba-Jobin Yvon, Inc. Japan). Intrinsic and extrinsic fluorescence was determined. For intrinsic fluorescence was used a 1 $g.L^{-1}$ sample solution, and analysis were made with an excitation wavelength of 280 nm in order to determine the intrinsic fluorescence by exciting the aromatic pool and amino acids present in the protein. The emission from 290 nm to 450 nm was collected (Rodrigues et al., 2020).

Extrinsic fluorescence was determined by adding the 8-Anilino-1-naphthalenesulfonic acid (ANS). ANS solution was previously prepared in methanol with a concentration of 1.5 mM and was stored protected from the light at 4 °C. ANS added to the protein allows access to the protein's hydrophobic sites. ANS was added to the protein solution until a final concentration of 75 µM and then was left to stabilize for 30 minutes at room temperature (~22 °C). After that, ANS – protein complex fluorescence was analyzed at an excitation wavelength of 370 nm, and the emission spectra were collected from 400 nm to 650 nm.

2.7 Thermogravimetric analyzes (TGA)

TGA was performed using a Shimadzu TGA 50 (Shimadzu Corporation, Kyoto, Japan). Each sample, with a weight of around 10 mg, was placed in the equipment crucible on top of the balance system. Samples were heated from 25 °C to 600 °C, with a heating rate of 10 °C.min^{-1}, under a nitrogen atmosphere. For each sample, at least two repetitions were made.

2.8 Iron quantification by Inductively coupled plasma-optical emission spectrometer – ICP-OES

The total iron content in LF was measured by using the equipment ICP, the analysis conditions were based on the work of Majka et al. (2013) and Martins et al. (2016). To digest LF-iron samples, 0.5 g of each sample was added to 9.5 mL to HNO_3 65%, with the exception of NSD80_100_2.8 in which was used 0.2 g with 9.8 mL of HNO_3 (this sample was very reactive and with a quantity of 0.5 g the reactor was unstable). Samples were then digested using the Microwave Digestion System SpeedWave4 (Berghof, Germany) with the following conditions 99 kW power, 15 min ramp, followed by a 20 min hold with a rate of 0.4 bar s^{-1} up to 50 bar, at 220 °C. Then samples were diluted until a concentration of HNO_3 of 2% was obtained.

Iron content in each digested sample was determined with the ICP technique using the equipment Spectrometer ICPE-9000 (Shimadzu, Japan) with the following conditions: plasma viewing mode was radial and the wavelength used to quantify the iron was 238.204 nm. Also, before sample analyzes, a calibration curve (0 mg.L^{-1}; 0.025 mg.L^{-1}; 0.05 mg.L^{-1}; 0.1 mg.L^{-1}; 0.5 mg.L^{-1}; 0.75 mg.L^{-1}; 1 mg.L^{-1}) was made. The measurement unit of the total released iron concentration is mg.L^{-1}.

2.9 Attenuated total reflectance Fourier transform infrared spectroscopy (ATR-FTIR)

ATR-FTIR analyzes were made to the LF powder of the native form, after NSD and after iron addition and NSD process. FTIR analyzes were performed using an ALPHA II- Bruker spectrometer (Ettlingen, Germany) in the wavelength region between 4000 and 400 cm^{-1}, at a resolution of 4 cm^{-1}, and 64 scans were conducted for each sample. Each spectrum was baseline corrected and the absorbance was normalized.

2.10 Iron release at different pH

The behavior of iron-loaded protein-based carriers was evaluated in different media, simulating the pH during gastrointestinal digestion, and for that, release tests were performed at pH 2 and 7.4 to mimic the stomach and intestinal pH, respectively. 2.86 g of NSD80_100_1.4 LF particles

(corresponding to 4 mg of iron) were placed in SpectraPor® Biotech dialysis membrane with a porosity of 500 Da (Repligen, Massachusetts, USA) previously washed with ultra-pure water. The dialysis membranes with the particles were placed in jacketed reactors with a temperature of 37 °C with two different media, an acidic medium of HCL-KCL buffer with a pH=2, and phosphate buffered saline (PBS) medium with a pH=7.4. To avoid bacterial spoilage, 2 $mg.mL^{-1}$ of sodium azide was added to each medium. Membranes with the particles inside were placed in the mediums and 500 µL was taken at defined time intervals.

Collected samples from the release tests were diluted until a final volume of 5 mL with HNO_3 2% (v/v), filtrated with nylon syringe filters, and analyzed by ICP, as described above, to quantify the iron release during the time in two different media.

2.10.1 Mathematical modelling

An equation that considers both Fickian and Case II transport (linear superposition model – LSM) effects in hydrophilic matrices was used to evaluate iron release from LF carriers (Berens & Hopfenberg, 1978):

$$M_t = M_{t,F} + M_{t,R} \qquad \text{(Eq. 1)}$$

where $M_{t,F}$ represents the contributions for the Fickian process and $M_{t,R}$ the contributions of the relaxation process, at time t (in minutes). Variable M_t is the overall mass released (mg) from the polymeric structure. This equation can be simplified using the first term Taylor series, resulting in equation 2 where M_F is the compound released at equilibrium and K_F is the Fickian diffusion rate constant:

$$M_{t,F} = M_F[1 - \frac{6}{\pi^2}\exp(K_F\, t)] \qquad \text{(Eq. 2)}$$

The swelling capacity of the polymer controls the polymer relaxation. Moreover, this is correlated to the dissipation of stress caused by penetrant input, expressed as a distribution of relaxation times, each assuming a first-order-type kinetic equation (Berens & Hopfenberg, 1978):

$$M_{t,R} = \sum_i M_{\infty,R_i}[1 - \exp(-K_{R_i}.\, t)] \qquad \text{(Eq. 3)}$$

with M_{∞,R_i} and K_{R_i} representing the contribution of the relaxation processes to compound release and the relaxation rate constants, respectively. When assuming a single major polymer relaxation that influences release, i=1, equation 3 can be simplified as follows:

$$\frac{M_f}{M_\infty} = M_f[1 - \frac{6}{\pi^2}\exp(-K_F\, t)] + (1 - M_R)[1 - \exp(-K_R t)] \qquad \text{(Eq 4)}$$

where M_f represents the fraction of the compound released by the Fickian process and M_R is the fraction of the compound released by the relaxation process. Thus, equation 4 can be used to characterise LSM for iron release from LF carriers.

This model can be used to represent pure Fickian, anomalous (i.e. Fickian and polymer relaxation phenomena), and Case II (only polymer relaxation phenomena) release processes in biopolymeric matrices. Eq. (2) (Fick's second law) and Eq. (4) (LSM) were applied to the experimental data to determine the release mechanism involved in the iron release from LF carriers at pH 2 and 7.4.

2.11 Statistical analysis

The data were fitted to Equation 2 and Equation 4 by non-linear regression, using the software STATISTICA v7.0 (Statsoft. Inc, USA).

For the purpose of minimizing the least squares function, the Levenberg-Marquadt method was applied. The determination coefficient, $Radj^2$, the squared root mean square error, *RMSE* (i.e., the square root of the sum of the squared residues (*SSE*) divided by the regression degrees of freedom), and residuals visual inspection for randomness and normality were used to assess the quality of the regressions. $Radj^2$ and *SSE* values were obtained from the software. The Standardised Halved Width (*SHW%*), which was defined as the ratio between the 90% Standard Error (also obtained from the software) and the value of the estimate, was used to assess the precision of the estimated parameters.

Software Origin 9.0 (OriginLab Corporation, Northampton, MA, USA) was used to perform sample analysis of variance (ANOVA), followed by multiple comparisons by the Tukey test ($p<0.05$).

3. Results and discussion

3.1 Unloaded carrier characterization

3.1.1 Particle size and morphology

Table 1 presents the size distribution of particles obtained at different drying temperature (60 ºC, 80 ºC, and 100 ºC) and concentrations (10 mg.mL^{-1}, 50 mg.mL^{-1}, and 100 mg.mL^{-1}), being represented as NSDtemperature_concentration (e.g., NSD60_10). SEM images and size distribution histogram are presented in Figure S1.

<Insert Table 1 here>

SEM images (Figure S1) show that particles' sizes and morphologies change according to the conditions used. The particles for the drying temperature of 60 °C and a concentration of 10 mg.mL^{-1} present a mean size of 1.103 ± 0.588 µm (Table 1). Most of the obtained particles in these conditions have a round surface, but there are some particles wrinkled, and others with holes and doughnut-shape (Figure S1A). The particles produced with 50 mg.mL^{-1} of LF at 60 °C present a mean size of 0.944 ± 0.470 µm and a round shape and smooth surface, but there are some particles with a doughnut-shape (Figure S1B). The doughnut shape particles can be explained by the formation of glassy skin in the early stage of the drying process of solution droplets (Arpagaus et al., 2017; Lee et al., 2011). This behavior was also observed by Lee et al. (2011) in particles produced using bovine serum albumin (BSA). Also, using 60 °C but with a concentration of 100 mg.mL^{-1} of LF, we obtained particles with a mean size of 0.925 ± 0.465 µm, but in this case, all the obtained particles have a round shape and a smooth surface (Figure S1C).

The particles produced with a drying temperature of 80 °C resulted in particles with a round shape and a smooth surface, and just few particles with holes and doughnut-shape were obtained in the particles produced with a concentration of 10 mg.mL^{-1} and 50 mg.mL^{-1}. The particles presented a mean size of 0.907 ± 0.453 µm, 0.812 ± 0.433 µm, 1.084 ± 0.550 µm for the concentrations of 10 mg.mL^{-1}, 50 mg.mL^{-1} and 100 mg.mL^{-1} (Figures S1D, S1E, S1F), respectively.

When the NSD was performed at 100 °C the obtained particles presented different morphologies for each LF concentration. For the lower LF concentration (10 mg.mL^{-1}) the particles presented a mean diameter of 0.677 ± 0.359 µm (Figure S1G). In this case, the particles have a wrinkled surface, due to the solution's low concentration and the high drying temperature, which immediately dries the solution droplets producing hollow particles (Arpagaus et al., 2017; Nandiyanto & Okuyama, 2011). When a concentration of 50 mg.mL^{-1} was used, the particles presented a mean size of 0.905 ± 0.516 µm, a round shape, and smooth surface morphology, with the presence of very few particles with holes (Figure S1H). Finally, the concentration of 100 mg.mL^{-1} produced particles with a round shape and a smooth surface, presenting a mean diameter of 1.184 ± 0.541 µm (Figure S1I).

These results agree with the work of Lee et al. (2011) that studied the effect of BSA protein concentration (5 mg.mL^{-1}, 10 mg.mL^{-1}, and 20 mg.mL^{-1}) on the particles obtained by spray drying. The authors concluded that the increase in protein concentration resulted in more smooth surface particles. They also noticed that drying temperature has a minimal influence on the particles' morphology (Lee et al., 2011). Similar conclusions were obtained by the laboratories Büchi that observed the same behavior for BSA with a concentration of 1 mg.mL^{-1}, 10 mg.mL^{-1}, and 100 mg.mL^{-1} (Büchi, 2017). Also Harsha et al. (2017) obtained similar results using albumin.

They concluded that particle size and size distribution increase with the protein concentration in the feed solution (Büchi, 2017; Harsha et al., 2017).

3.1.2 Circular dichroism

3.1.2.1 Secondary structure

The circular dichroism analysis in the Far-UV region (185 – 260 nm) was used to study the conformational changes in the protein secondary structure after the drying process. The analysis was based on the characteristic CD spectrum of the helices, β-sheet, and random coils CD spectrum obtained for the protein secondary structure, providing an estimation of the LF secondary structure composition after the drying process. The CD study can be used to evaluate quantitatively the overall secondary structure content of the protein since the different forms of regular secondary structure found in proteins exhibit distant spectra (Kelly & Price, 2005). Obtained spectrum for each LF condition is represented in Figure 1a).

LF Native (LF Nat) profile shows a negative peak at 208.5 nm, representing a weak but broad $n \rightarrow \pi^*$ transition, which represents the α-helix configuration and is in agreement with other works (Nunes et al., 2020; Wang et al., 2017a, 2017b). Also, it presents a positive and intense peak at 190 nm and a slight peak at 215 nm, representing β-sheet components.

The samples dried in NSD at different temperatures have a very similar spectra shape, even when compared with the control (LF Nat), and no shifts were observed. However, ellipticity differences were noticed at 208.5 nm in the CD spectra of the NSD samples, with an ellipticity decrease when compared with the LF Nat. These differences are even more evident for the NSD samples at the higher concentration (100 $mg.mL^{-1}$). The same behavior was obtained at 190 nm for the samples with a higher concentration of LF and dried at higher temperatures (NSD80 and NSD100) which present higher ellipticity. These results can be related to the formation of small protein aggregates during the NSD process. Similar results were obtained by Wang et al. (2017b) when LF dried using single droplet drying to simulate the spray drying process. Other work corroborates that these changes in the spectra can be related to protein aggregation. Brisson et al. (2007) studied LF aggregation in aqueous solutions with different temperatures and showed that LF Nat is heat sensitive and at 60 °C can form intermolecular disulphide linkages resulting in protein aggregates (Brisson et al., 2007; Zhang et al., 2015).

Obtained results show that the drying process using the NSD B-90 HP with temperatures of 60 °C, 80 °C, and 100 °C did not cause major changes in the secondary structure of the LF protein since all the characteristics of the structures were maintained,. Although, during NSD, especially for higher temperatures (80 °C and 100 °C) can be formed intermolecular disulphide linkages, resulting in small changes on protein conformation.

<Insert Figure 1 here>

3.1.2.2 Tertiary structure

The tertiary structure spectra can be evaluated in the region between 260 nm to 320 nm, which assesses the aromatic amino acids. Each amino acid has a characteristic wavelength: the tryptophan (Trp) with a peak between 290 and 300 nm, the tyrosine (Tyr) that shows a small peak between 280 nm and 290 nm, and the phenylalanine (Phe) with a peak between 255 nm and 270 nm, and by their analysis is possible to identify changes in the protein tertiary structure (Kelly et al., 2005). Figure 1b) presents the tertiary structure spectrum obtained by circular dichroism for the LF native and for LF after the NSD process at different temperatures.

Comparing LF Native spectrum with the obtained spectra for dried samples, it is possible to observe that there are no major differences in obtained results. The peaks are in the same wavelength range for all samples, meaning that NSD process did not cause major changes in the protein amino acids and the protein tertiary structure. However, in the Tyr peak, between 280 and 290 nm, there is a slight difference in the peak intensity. Samples after the drying process have an increase in the intensity peak when compared with the LF Nat. This behavior is more evident for the NSD80_10 and NSD100_10. This result is in agreement with the results obtained by other authors that reported changes in the Tyr peak after the heating process (Liu et al., 2016; Xu et al., 2019), which related them to small conformational changes due to the drying process and consequent small aggregation formation (Brisson et al., 2007).

3.1.3 Electrophoresis

SDS-Page electrophoresis (Figure S2) was performed in order to evaluate potential changes in the molecular structure and size of the LF after the drying process. The native form of LF (band A) and samples dried with NSD process (bands B to J) present a major band that corresponds to LF molecular mass (75 kDa).

After the NSD process (60 °C, 80 °C, and 100 °C) there are no changes in the intensity of the major protein band, which suggests that there is no major molecular degradation of LF when dried in the NSD. Although for the samples NSD60_50, NSD60_100, NSD80_50, NSD80_100, NSD100_50, and NSD100_100, a minor band was obtained around 50 kDa and 30 kDa, which suggests a minor molecular degradation of LF occurred to the NSD process. The slight band at 30 kDa can be due to residual α-lactalbumin, while the band around 50 kDa can be due to αs2-casein residues (Wang et al., 2017a). The small aggregations described above are not evident in

the electrophoresis because they probably were broken in the presence of SDS (Brisson et al., 2007).

3.1.4 Thermogravimetric analysis (TGA)

TGA provides information about the thermal degradation of the samples. Table S1 presents the thermal events and respective weight loss of the samples. The thermal profile of each sample is presented in Figure 2.

LF samples dried at different temperatures presented two major thermal degradation events. The first one occurred between 27 °C and 145 °C and the other one between 150 °C and 500 °C. The weight loss of the first thermal event can be attributed to water evaporation. The LF Nat sample presents a higher weight loss (9.42 ± 0.13%) while the sample dried at 60 °C presents a weight loss of 7.82 ± 0.67%, and the ones dried at NSD80 and NSD100 result in a weight loss of 6.10 ± 0.16% and 5.33 ± 0.12%, respectively. Lower weight loss was obtained for the high drying temperature (100 °C), which shows that the use of higher temperatures during the NSD are more effective in lowering the samples' moisture.

In the second event, between 150 °C and 500 °C, all the samples have a high weight loss that can be attributed to protein degradation, i.e., degradation of the polypeptide structure. The similar extent of mass loss in drying temperatures of 80 °C (60.90 ± 2.11%) and 60 °C (59.89 ± 0.07%) and in LF Nat (59.05 ± 0.41%) indicates that the primary pyrolysis products of these two samples are similar. Although the NSD 100 °C has a higher weight loss (63.82 ± 0.41%), which can be observed in the derivative curve, it shows a degradation peak at a higher temperature than the other samples. This difference shows that LF dried at 100 °C is slightly more resistant to thermal degradation than LF dried at 60 °C and 80 °C. This result indicates that drying LF at 60°C and 80 °C in NSD did not have an effect on the protein degradation, but 100 °C had. This behavior can be related to the formation of non-covalently linked oligomers and therefore intermolecular thiol/disulphide and non-covalent interactions during the drying process that can be more evident at 100 °C. Since this temperature is higher than the LF denaturation temperature, more bond cleavage and new interactions can be formed, resulting in a more resistant structure (Brisson et al., 2007).

Results are in agreement with Bourbon et al. (2020), which concluded that NSD drying temperature affects protein degradation, having more thermal degradation in higher NSD temperatures. Results suggest that NSD drying temperature can have a small effect on protein conformation.

<Insert Figure 2 here>

3.2 Iron-loaded carriers characterization

After testing different drying conditions and studying the effect of three drying temperatures on the protein structure, a drying temperature of 80 °C and a LF concentration of 100 mg.mL^{-1} were selected to develop the carrier of the mineral iron. The selection was based on particle morphology, since at 80 °C the particles have a round shape and smooth surface. Particles with holes and doughnut shapes were avoided since particles with this morphology have higher specific surface when compared to spherical shape particles (Arpagaus et al., 2017). Based on the obtained TGA results, for the drying temperature of 100 °C there is a higher weight loss which can be related to conformation changes in the protein. Furthermore, samples dried at 80 °C present lower moisture content that the ones dried at 60 °C.

3.2.1 Particles size and morphology

Figure 3 presents the SEM images of samples loaded with different iron concentrations and Table 2 presents the size distribution for each sample. Results show particles with a round shape and a smooth surface. The loaded particles have an average size similar to the control NSD80_100 (1.084 ± 0.550 µm) with particles size of 1.018 ± 0.576 µm, 0.903 ± 0.492 µm and 0.987 ± 0.574 µm for NSD80_100_0.7, NSD80_100_1.4, and NSD80_100_2.8, respectively. Iron addition did not cause changes in the obtained particles' morphology, shape, and size.

<Insert Figure 3 and Table 2 here>

3.2.2 Circular dichroism

Figure 4a) shows that the samples' spectra presented the same shape, with a typical CD signal of the LF. The obtained spectrum has the characteristic peaks of 190 nm and also a small peak at 215 nm, which correspond to the β-sheet and at 208.5 nm, which is related to the fingerprint of α-helix.

Comparing the obtained spectrum for the control sample, NSD80_100, and the samples with iron additions, there are just small differences in the ellipticity that can be due to small conformation changes in the protein to bind to the mineral iron (Brisson et al., 2007).

<Insert Figure 4 here >

Similar results were reported by Bokkhim et al. (2014), who obtained a spectrum with only minor differences in magnitude for different iron concentrations in LF, supporting the fact that the binding of iron to LF does not cause major secondary structure changes.

Figure 4b) shows the tertiary structure spectrum for the protein in its native form, after NSD process at 80 °C, and after iron addition in different concentrations. Similar to the results reported above, all samples maintained the characteristic peaks of each amino acid. Although, for samples with iron addition, a higher intensity for the Trp and Phe peaks is obtained. These results are similar to the results obtained by Bokkhim et al. (2014) where LF samples without or with lower iron concentration present a negative ellipticity for the Trp peak, while iron addition resulted in a positive ellipticity in the same wavelength range. The change in the Trp peak is related to conformational changes in the neighbor amino acids (Tyrosine, Tyrosine, Histidine, and Asparagine) that allow the LF to bind to the mineral iron (Wang et al., 2019).

3.2.3 Visible CD (300 nm – 600 nm)

CD in the visible range (Vis-CD) (300 nm – 600 nm) allows evaluating the interaction between a protein and a metal ion. Vis-CD spectra of transition metal ions are a result of a mixture of absorption bands resulting from d-d electronic transitions. At these wavelengths, Vis-CD spectrum is only obtained when the metal ion is in a chiral environment (Albetel & Outten, 2019; Stanyon et al., 2014).

<Insert Figure 5 here>

Figure 5 shows the spectrum obtained for visible CD from 300 nm to 600 nm for the control samples without iron addition and LF with three different iron concentrations. The obtained spectra for LF Nat and NSD80_100 have a slightly positive peak at 334 nm and a slightly negative peak at 448 nm. Although samples with iron addition have a different spectrum, in this case, was obtained an intense positive peak at 330 nm, and an intense negative peak that increases with the iron concentration, at 451 nm, 449.5 nm, and 448 nm for NSD80_100_0.7, NSD80_100_1.4, and NSD80_100_2.8, respectively. Additionally, there is a difference between the spectrum with different iron concentrations. The samples with lower iron concentration have a shoulder at 306 nm and the samples with higher iron concentration present a peak at 306 nm. These results show that iron concentration leads to differences in the obtained spectrum. Also, the obtained results confirmed the presence of an LF-iron interaction. Results are in accordance with the results obtained by Bokkhim et al. (2014) which obtained a good correlation between the iron content and the change in the samples' spectra.

3.2.4 Electrophoresis

Results are very similar to those obtained after the NSD process reported in section 3.1.3. Iron addition did not cause changes in the intensity of the major protein band, which suggests that

there is no molecular degradation of LF when it is bonded to the mineral iron (Figure S3). Similar results were obtained by Wang et al. (2017b), where different iron concentrations did not cause LF degradation.

3.2.4. TGA

TGA analyzes were performed to evaluate the effect of iron addition on the thermal stability of LF Nat and LF with different iron concentrations. The mass loss patterns and derivatives obtained by thermogravimetric analysis of three forms of LF are presented in Figure 6. The first weight loss event was until 145 °C, corresponding to moisture loss, are very similar for the three iron concentrations, 7.04 ± 0.02%, 7.10 ± 0.07%, and 6.89 ± 0.66%, to the samples NSD80_100_0.7, NSD80_100_1.4, and NSD80_100_2.8, respectively. These results are explained by the drying temperature that was the same for all the samples, showing the water content in the samples after the drying process is very similar.

After 150 °C and until 500 °C the weight loss in all the samples started to drop, which indicates the degradation of polypeptide structure. The samples with NSD80_100_0.7 present the minimum peak in the derivative at a lower temperature, at 323.58 °C compared with the 328.9 °C and 331.3 °C from the NSD80_100_1.4 and NSD80_100_2.8, respectively. The results show that LF with higher concentrations of iron are more resistant due to the compact conformation of LF bound with iron (Wang et al., 2017b).

<Insert Figure 6 here>

3.2.5. Intrinsic and extrinsic fluorescence

Changes in protein structure imposed by iron addition and the NSD process were assessed using fluorescence spectroscopy of endogenous tryptophan. For that, two different ligand binding studies were made, one with ANS to study the protein extrinsic fluorescence, and other where protein intrinsic fluorescence was analyzed. The NSD process and iron addition decreased Trp fluorescence intensity, which is more evident for higher iron concentrations. When compared with the LF Nat, the NSD80_100 sample has less fluorescence intensity but no shift in the fluorescence maximum was detected (328.77 nm), indicating that the NSD process does not cause changes in the Trp microenvironment, and therefore the decrease in fluorescence observed must be the result of an increased quenching of the neighbor amino acids due to small conformation rearrangements or higher structural dynamics (Bhattacharjee & Das, 2000; Lakowicz, 2006; Rodrigues et al., 2020).

Figure 7a) shows that fluorescence intensity decreases with iron addition, which is more evident for higher iron concentrations. The intensity goes from 15762 a.u. in the LF Nat, to 4269.88 a.u. in the sample of LF with higher iron concentration. This decrease can be a result of an increased quenching from the neighbor amino acids, which results from conformational rearrangements due to iron binding (Brisson et al., 2007; Rodrigues et al., 2020). Also, there is a red-shift in the maximum of Trp fluorescence with a broadening of the spectra to the right with the increase of iron concentration, from 328.77 nm in the samples without iron, to 329.9, 332.19 and 333.33 nm for the samples NSD80_100_0.7, NSD80_100_1.4, and NSD80_100_2.8, respectively. Corresponding to a maximum red-shift of 4.56 nm, which indicates that tryptophan was exposed to a more hydrophilic environment, which is justified by the conformational changes in the protein when it binds to iron. Protein structure without iron is less stable and less compact when compared with the LF-iron complex, which results in a more closed structure (Wang et al., 2013).

Similar results were obtained by Wang et al. (2013) that analyzed the effect of different iron saturation (1%, 9%, 38%, 58%, and 96%) on the LF fluorescence, and observed that there is an intensity decrease and a wavelength increase (red-shift) for lower concentrations of iron. These results corroborate the occurrence of substantial structural changes resulting in different Trp local environment and solvent accessibility.

<Insert Figure 7 here>

The obtained emission spectra for ANS-LF complex are presented in Figure 7b). Results show an intensity decrease and a small blue-shift for the sample with a higher concentration of iron; while for other samples no shifts are observed. Results obtained for LF Nat and LF after NSD process present the same behavior. Iron addition leads to a decrease in fluorescence and a blue-shift (1.17 nm) for the sample NSD80_100_2.8. Samples with iron addition display lower fluorescence intensities than the samples without iron addition resulting from a lower affinity to ANS. The decrease in ANS fluorescence may arise from a decreased binding affinity or from less exposure to hydrophobic regions due to higher structural changes caused by iron binding and hydrophobic pocket occlusion. From the results can be concluded that the increase in iron concentration leads to fewer places available for the ANS to bind to the protein. This behavior results from a conformational change in the protein caused by iron binding, also observed by tertiary structure analysis by CD.

3.2.6. Fourier Transform Infrared spectroscopy (FTIR)

Figure 8 shows the obtained spectra for samples with and without iron addition. LF Nat spectrum shows the characteristic protein absorption peaks, the amide I at 1637 cm^{-1} due to the C=O

546 stretching vibration of the peptide group, and the amide II at 1525 cm^{-1} due to N-H bending with
547 a contribution of C-N stretching vibrations. The absorbance peak at 3258 cm^{-1} represents the O-
548 H stretching, indicating the presence of water in the sample; this peak has a lower intensity in
549 samples that were dried in the NSD when compared with the LF Nat, which is in agreement with
550 the obtained results for TGA.

551 <Insert Figure 8 here>

552 The peaks observed between 2800-3000 cm^{-1} are related to C-H stretching vibration,
553 corresponding to the symmetrical and asymmetrical stretching in the $–CH_2$ and $–CH_3$ groups
554 (Martins et al., 2016). The peak that corresponds to amide I observed at 1637 cm^{-1} region gives
555 information about the protein secondary structure, and shows no shifts and changes in the amide
556 I and consequently in the protein secondary structures (Duca et al., 2018; Martins et al., 2016).
557 Regarding the amide II peak, observed at 1525 cm^{-1} for the LF Nat, starts to differentiate into two
558 peaks for the NSD samples with higher drying temperatures (NSD80 and NSD100), obtained one
559 peak at 1522 cm^{-1} and another at 1540 cm^{-1}. The differences in amide II peak were also obtained
560 by the author Wang et al. (2017a) for spray dried LF particles at 70 °C and 95 °C.

561 The observed band around 1064 cm^{-1} is assigned to N≡C or C=C stretch and C-H deformation
562 vibrations of tryptophan (Duca et al., 2018). The obtained results show a small shift in the Trp
563 peak, from 1063 cm^{-1} in the LF Nat for 1065 cm^{-1} for samples after the NSD process and to
564 1066 cm^{-1} after iron addition. These results can be related to small protein conformation
565 rearrangement as described before in the secondary and tertiary protein structure and fluorescence
566 analysis.

567 The spectrum obtained for each sample shows they all have the typical protein bands, and only
568 small shifts in the peaks were obtained. These results are in agreement with the results obtained
569 by Martins et al. (2016) and Wang et al. (2017a) that obtained only small shifts in amide II
570 observed by FTIR after LF-iron particles production and LF particles by spray drying,
571 respectively

572 3.2.7. Iron release in different pH

573 The behavior of iron-loaded carriers was evaluated at two different pH (2 and 7.4). They can give
574 information about the behavior of the carrier in the gastrointestinal tract (e.g., stomach and small
575 intestine) but also in acidic and neutral foods (Martins et al., 2016; Nunes et al., 2020).
576 Figure 9a) shows the iron release from LF particles at pH 2 and pH 7.4, at 37 °C. Results show
577 that at pH 7.4 there is no iron release, while at acidic pH the iron is released from the LF particles.

At pH 7.4 the LF remains bounded to iron, indicating a good capacity of LF to keep its structure and bound to iron at neutral pH. On the other hand, at pH 2, the LF structure starts to denature, and iron starts to be released from the carrier because at these conditions, the pH is very different from 8.5, the LF's isoelectric point. This behavior was described by Baker & Baker, (2004), that analyzed the pH dependence of the iron release process from LF and concluded that LF retains iron at pH ~3.0, while at pH 7 there is no iron release. The results are in agreement with the results obtained by Martins et al. (2016) that analyzed the iron released from LF gels at similar pH.

<Insert Figure 9 here>

In order to evaluate the mechanism of iron release from the particles, the data were fitted to Fick's second law (Eq. 2) and LSM (Eq. 4). Results are represented in Figure 9b), where are presented the experimental values and the Fick's fitting and the LSM fitting for iron release at pH 2. At neutral pH, there is no iron released, which makes it impossible to apply these models. The values for Fick's constant and relaxation constant are presented in Table S2. Results show that Fick's model does not fit the experimental data and consequently does not describe the iron release mechanism at pH 2 (Figure 9b)). However, LSM adequately fits the experimental data ($Radj^2$=0.9879). The value of M_R was 21.5627 mg, which means that polymer relaxation (Case II transport) was the major release mechanism responsible for the iron release. In the case of Fick's mechanism (diffusion mechanism), it was obtained a M_f of 0.0349 mg of iron was released. The relaxation rate constant (K_R) is lower than the Fickian rate constant (K_F) showing that iron is released more rapidly by Fick's diffusion than by polymer relaxation (Martins et al., 2016). Results show that the release mechanism for iron-loaded protein-based carriers can be described by the LSM model. Thus, the iron released comes from a combination of diffusion and macromolecular swelling processes confirming that LF-iron particles are a hydrophilic and swellable system.

4. Conclusions

With this work, it is possible to conclude that NSD is an alternative technology to obtain dried and stable LF particles. Despite being used at high temperatures, this process does not denature the protein as proved by CD analysis and SDS-page electrophoresis results. Only small ellipticity changes were obtained in the secondary and tertiary structure CD analysis, probably due to small formed aggregations in the protein. This technology allows the production of round shape and smooth surface particles with sizes ranging from 38.8 nm to 4533.6 nm.

Iron addition does not cause protein degradation as observed in the obtained results for the secondary structure analysis by CD, but leads to changes in protein conformation as proved by

the results obtained in the tertiary structure that shows higher ellipticity for Trp peak. Fluorescence results are also in agreement with obtained results for tertiary structure in CD, which shows that iron binds to LF, causing conformational changes in the neighbor amino acids. LF-iron interaction was also confirmed by Vis-CD.

Stability tests at pH 2 and pH 7.4, show that LF-iron carries are stable at neutral pH, and no iron is released in this condition. On the other hand, at pH 2, the iron is released over time and polymer relaxation is the governing phenomenon.

This work presents promising results for the use of NSD technology for the development of iron delivery systems aiming the development of fortified foods, showing a simple, easy, and quick technology for dried particle production suitable even for temperature-sensitive materials like proteins.

Acknowledgements

The author Arlete M. Marques (SFRH/BD/132911/2017) is the recipient of a fellowship from Fundação para a Ciência e Tecnologia (FCT, Portugal). This study was supported by the Portuguese Foundation for Science and Technology (FCT) under the scope of the strategic funding of UIDB/04469/2020 unit, and by LABBELS – Associate Laboratory in Biotechnology, Bioengineering and Microelectromechanical Systems, LA/P/0029/2020. The authors would like to acknowledge Formulab (Maia, Portugal) for the iron samples and Juliana Sousa from International Iberian Nanotechnology Laboratory (INL) for helping with the ICP analysis. We also would like thank to the Advanced Electron Microscopy, Imaging, and Spectroscopy (AEMIS) from INL for their support.

5. References

Albetel, A.-N., & Outten, C. E. (2019). Characterization of glutaredoxin Fe-S cluster binding interactions using circular dichroism spectroscopy. *Methods Enzymol*, *599*, 327–353. https://doi.org/10.1016/bs.mie.2017.11.003

Arpagaus, C. (2019a). PLA/PLGA nanoparticles prepared by nano spray drying. *Journal of Pharmaceutical Investigation*, *49*(4), 405–426. https://doi.org/10.1007/s40005-019-00441-3

Arpagaus, C. (2019b). Production of food bioactive-loaded nanoparticles by nano spray drying. In S. M. Jafari (Ed.), *Nanoencapsulation of Food Ingredients by Specialized Equipment* (Volume 3, Issue November, pp. 151–211). Academic Press (Elsevier Inc.). https://doi.org/10.1016/B978-0-12-815671-1.00004-4

Arpagaus, C., John, P., Collenberg, A., & Rutti, D. (2017). Nanocapsules formation by nano

spray drying. In S. M. Jafari (Ed.), *Nanoencapsulation Technologies for the Food and Nutraceutical Industries* (pp. 346–401). Academic Press.

Baker, H. M., & Baker, E. N. (2004). Lactoferrin and Iron : structural and dynamic aspects of binding and release. *BioMetals*, *17*, 209–216. https://doi.org/10.1023/b:biom.0000027694.40260.70

Berens, A. R., & Hopfenberg, H. B. (1978). Diffusion and relaxation in glassy polymer powders: 2. Separation of diffusion and relaxation parameters. *Polymer*, *19*(5), 489–496. https://doi.org/https://doi.org/10.1016/0032-3861(78)90269-0

Bhattacharjee, C., & Das, K. P. (2000). Thermal unfolding and refolding of β-lactoglobulin. *European Journal of Biochemistry*, *267*(13), 3957–3964. https://doi.org/https://doi.org/10.1046/j.1432-1327.2000.01409.x

Bokkhim, H., Bansal, N., GrØndahl, L., & Bhandari, B. (2013). Physico-chemical properties of different forms of bovine lactoferrin. *Food Chemistry*, *141*(3), 3007–3013. https://doi.org/https://doi.org/10.1016/j.foodchem.2013.05.139

Bokkhim, H., Tran, T., Bansal, N., Grøndahl, L., & Bhandari, B. (2014). Evaluation of different methods for determination of the iron saturation level in bovine lactoferrin. *Food Chemistry*, *152*, 121–127. https://doi.org/10.1016/j.foodchem.2013.11.132

Bourbon, A. I., Barbosa-Pereira, L., Vicente, A. A., Cerqueira, M. A., & Pastrana, L. (2020). Dehydration of protein lactoferrin-glycomacropeptide nanohydrogels. *Food Hydrocolloids*, *101*, 105550. https://doi.org/https://doi.org/10.1016/j.foodhyd.2019.105550

Bourbon, A. I., Pinheiro, A. C., Carneiro-da-Cunha, M. G., Pereira, R. N., Cerqueira, M. A., & Vicente, A. A. (2015). Development and characterization of lactoferrin-GMP nanohydrogels: Evaluation of pH, ionic strength and temperature effect. *Food Hydrocolloids*, *48*, 292–300. https://doi.org/10.1016/j.foodhyd.2015.02.026

Brisson, G., Britten, M., & Pouliot, Y. (2007). Heat-induced aggregation of bovine lactoferrin at neutral pH: Effect of iron saturation. *International Dairy Journal*, *17*(6), 617–624. https://doi.org/10.1016/j.idairyj.2006.09.002

Büchi, L. (2017). Sub-micron Bovine Serum Albumin particles. In *Application Note No. 272/2017* (Issue 272).

Büchi Labortechnik AG. (2017a). *Nano Spray Dryer B-90 HP*. Büchi. https://www.buchi.com/en/products/spray-drying-and-encapsulation/nano-spray-dryer-b-90-hp

Büchi Labortechnik AG. (2017b). *Nano Spray Dryer B-90 HP - Operation Manual*. https://static1.buchi.com/sites/default/files/downloads/093261_B-

90_Operation_Manual_en_0.pdf?6184640abe255f77115287bb82b78c058b6217b0

Churio, O., & Valenzuela, C. (2018). Development and characterization of maltodextrin microparticles to encapsulate heme and non-heme iron. *Lwt*, *96*(May), 568–575. https://doi.org/10.1016/j.lwt.2018.05.072

Duca, G., Anghel, L., & Erhan, R. V. (2018). Structural aspects of lactoferrin and serum transferrin observed by FTIR spectroscopy. *Chemistry Journal of Moldova*, *13*(1), 111–116. https://doi.org/10.19261/cjm.2018.482

Fathima, S. J., Nallamuthu, Ii., & Khanum, F. (2017). Vitamins and minerals fortification using nanotechnology: bioavailability and recommended daily allowances. In A. M. Grumezescu (Ed.), *Nutrient delivery* (pp. 457–496). https://doi.org/https://doi.org/10.1016/B978-0-12-804304-2.00012-3

Gharibzahedi, S. M. T., & Jafari, S. M. (2017). Nanoencapsulation of Minerals. In S. M. Jafari (Ed.), *Nanoencapsulation of food biactive ingredients*. https://doi.org/10.1016/B978-0-12-809740-3.00009-X

Goulding, D. A., O'Regan, J., Bovetto, L., O'Brien, N. M., & O'Mahony, J. A. (2021). Influence of thermal processing on the physicochemical properties of bovine lactoferrin. *International Dairy Journal*, *119*, 105001. https://doi.org/https://doi.org/10.1016/j.idairyj.2021.105001

Gupta, C., Chawla, P., Arora, S., Tomar, S. K., & Singh, A. K. (2015). *Food Hydrocolloids Iron microencapsulation with blend of gum arabic , maltodextrin and modi fi ed starch using modi fi ed solvent evaporation method e Milk forti fi cation*. *43*, 622–628. https://doi.org/10.1016/j.foodhyd.2014.07.021

Harsha, S. N., Al-dhubiab, B. E., Nair, A. B., Attimarad, M., Venugopala, K. N., & Kedarnath, S. A. (2017). Pharmacokinetics and tissue distribution of microspheres prepared by spray drying technique: targeted drug delivery. *Biomedical Research*, *28*(8), 3387–3396.

Harsha, S. N., Aldhubiab, B. E., Nair, A. B., Alhaider, I. A., Attimarad, M., Venugopala, K. N., Srinivasan, S., Gangadhar, N., & Asif, A. H. (2015). Nanoparticle formulation by Buchi B-90 nano spray dryer for oral mucoadhesion. *Drug Design, Development and Therapy*, *9*, 273–282. https://doi.org/10.2147/DDDT.S66654

Hatefi, L., & Farhadian, N. (2020). A safe and efficient method for encapsulation of ferrous sulfate in solid lipid nanoparticle for non-oxidation and sustained iron delivery. *Colloids and Interface Science Communications*, *34*(December 2019), 100227. https://doi.org/10.1016/j.colcom.2019.100227

Katouzian, I., & Jafari, S. M. (2016). Nano-encapsulation as a promising approach for targeted

714 delivery and controlled release of vitamins. *Trends in Food Science & Technology*, *53*,
715 34–48. https://doi.org/10.1016/j.tifs.2016.05.002

716 Katuwavila, N. P., Perera, A. D. L. C., Dahanayake, D., Karunaratne, V., Amaratunga, G. A. J.,
717 & Karunaratne, D. N. (2016). Alginate nanoparticles protect ferrous from oxidation:
718 Potential iron delivery system. *International Journal of Pharmaceutics*, *513*(1–2), 404–
719 409. https://doi.org/10.1016/j.ijpharm.2016.09.053

720 Kelly, S. M., Jess, T. J., & Price, N. C. (2005). How to study proteins by circular dichroism.
721 *Biochimica et Biophysica Acta - Proteins and Proteomics*, *1751*(2), 119–139.
722 https://doi.org/10.1016/j.bbapap.2005.06.005

723 Kelly, S., & Price, N. (2005). The Use of Circular Dichroism in the Investigation of Protein
724 Structure and Function. *Current Protein & Peptide Science*, *1*(4), 349–384.
725 https://doi.org/10.2174/1389203003381315

726 Lakowicz, J. (2006). *Principles of fluorescence spectroscopy* (3rd ed.). Springer US.

727 Lee, S. H., Heng, D., Ng, W. K., Chan, H. K., & Tan, R. B. H. (2011). Nano spray drying: A
728 novel method for preparing protein nanoparticles for protein therapy. *International*
729 *Journal of Pharmaceutics*, *403*(1–2), 192–200.
730 https://doi.org/10.1016/j.ijpharm.2010.10.012

731 Levay, P. F., & Viljoen, M. (1995). Lactoferrin: a general review. *Haematologica*, *80*(May
732 2014), 252–267. https://doi.org/https://doi.org/10.3324/%25x

733 Liu, F., Wang, D., Ma, C., & Gao, Y. (2016). Conjugation of polyphenols prevents lactoferrin
734 from thermal aggregation at neutral pH. *Food Hydrocolloids*, *58*, 49–59.
735 https://doi.org/10.1016/j.foodhyd.2016.02.011

736 Liu, F., Zhang, S., Li, J., McClements, D. J., & Liu, X. (2018). Recent development of
737 lactoferrin-based vehicles for the delivery of bioactive compounds : Complexes ,
738 emulsions , and nanoparticles. *Trends in Food Science & Technology*, *79*(June), 67–77.
739 https://doi.org/https://doi.org/10.1016/j.tifs.2018.06.013

740 Lozoff, B. (2007). Iron deficiency and child development. *Food and Nutrition Bulletin*, *28*(4
741 Suppl), S560-71. https://doi.org/10.1177/15648265070284S409

742 Majka, G., Klaudyna, S., Kurpiwaska, K., Heczko, P., Stochel, G., Strus, M., & Brindell, M.
743 (2013). A high-throughput method for the quantification of iron saturation in lactoferrin
744 preparations. *Analytical and Bioanalytical Chemistry*, *405*, 5191–5200.
745 https://doi.org/10.1007/s00216-013-6943-9

746 Marques, A. M., Azevedo, M. A., Teixeira, J. A., Pastrana, L. M., Gonçalves, C., & Cerqueira,
747 M. A. (2019). Engineered Nanostructures for Enrichment and Fortification of Foods. In G.

748 Molina, I. F. M. Pelissari, & A. M. Asiri (Eds.), *Food Applications of Nanotechnology* (pp.
749 61–86). CRC Press. https://doi.org/https://doi.org/ 10.1201/9780429297038-4.

750 Marques, A. M., Bourbon, A. I., Pastrana, L. M., Cerqueira, M. A., & Teixeira, J. A. C. (2021).
751 Nano Spray Drying for the Encapsulation of Bioactive Ingredients. In S. M. Jafari & A.
752 Rashidinejad (Eds.), *Spray Drying Encapsulation of Bioactive Materials* (1st ed., p. 29).
753 Taylor & Francis. https://www.taylorfrancis.com/chapters/edit/10.1201/9780429355462-
754 12/nano-spray-drying-encapsulation-bioactive-ingredients-arlete-maria-lima-marques-ana-
755 isabel-bourbon-lorenzo-pastrana-miguel-angelo-cerqueira-jose-antonio-couto-teixeira

756 Martins, J. T., Santos, S. F., Bourbon, A. I., Pinheiro, A. C., González-Fernández, Á., Pastrana,
757 L. M., Cerqueira, M. A., & Vicente, A. A. (2016). Lactoferrin-based nanoparticles as a
758 vehicle for iron in food applications – Development and release profile. *Food Research*
759 *International*, *90*, 16–24. https://doi.org/10.1016/j.foodres.2016.10.027

760 Menza, V., & Probart, C. (2013). *Eating well for good health* (FAO (ed.)).

761 Nandiyanto, A. B. D., & Okuyama, K. (2011). Progress in developing spray-drying methods for
762 the production of controlled morphology particles: From the nanometer to submicrometer
763 size ranges. *Avanced Powder Technology*, *22*, 1–19.
764 https://doi.org/https://doi.org/10.1016/j.apt.2010.09.011

765 Naveen, S., & Kanum, F. (2014). *Characterization and evaluation of iron nano-emulsion*
766 *prepared by high speed homogenization*. *3*(1), 45–55.

767 Nunes, R., Pereira, B. D., Cerqueira, M., Silva, P. M., Pastrana, L., Vicente, A. A., Martins, J.,
768 & Bourbon, A. I. (2020). Lactoferrin-based nanoemulsions to improve the physical and
769 chemical stability of omega-3 fatty acids. *Food & Function*, *11*(3), 1966–1981.
770 https://doi.org/10.1039/c9fo02307k

771 Oliveira, A. M., Guimarães, K. L., Cerize, N. N. P., Tunussi, A. S., & Poço, J. G. R. (2013).
772 Nano Spray Drying as an Innovative Technology for Encapsulating Hydrophilic Active
773 Pharmaceutical Ingredients (API). *Nanomedicine & Nanotechnology*.
774 https://doi.org/http://dx.doi.org/10.4172/2157-7439.1000186

775 Pedrozo, R. C., Antônio, E., Khalil, N. M., & Mainardes, R. M. (2020). Bovine serum albumin–
776 based nanoparticles containing the flavonoid rutin produced by nano spray drying.
777 *Brazilian Journal of Pharmaceutical Sciences*, *56*, 1–8. https://doi.org/10.1590/s2175-
778 97902019000317692

779 Percy, L., Mansour, D., & Fraser, I. (2017). Iron deficiency and iron deficiency anaemia in
780 women. *Best Practice and Research: Clinical Obstetrics and Gynaecology*, *40*, 55–67.
781 https://doi.org/10.1016/j.bpobgyn.2016.09.007

Pérez-Masiá, R., López-Nicolás, R., Periago, M. J., Ros, G., Lagaron, J. M., & López-Rubio, A. (2015). Encapsulation of folic acid in food hydrocolloids through nanospray drying and electrospraying for nutraceutical applications. *Food Chemistry*, *168*, 124–133. https://doi.org/10.1016/j.foodchem.2014.07.051

Rodrigues, R. M., Avelar, Z., Vicente, A. A., Petersen, S. B., & Pereira, R. N. (2020). Influence of moderate electric fields in β-lactoglobulin thermal unfolding and interactions. *Food Chemistry*, *304*(March 2019). https://doi.org/10.1016/j.foodchem.2019.125442

Sharma, R. (2019). *Chapter 17 - Whey Proteins in Functional Foods* (H. C. Deeth & N. B. T.-W. P. Bansal (eds.); pp. 637–663). Academic Press. https://doi.org/https://doi.org/10.1016/B978-0-12-812124-5.00018-7

Shubham, K., Anukiruthika, T., Dutta, S., Kashyap, A. V., Moses, J. A., & Anandharamakrishnan, C. (2020). Iron deficiency anemia: A comprehensive review on iron absorption, bioavailability and emerging food fortification approaches. *Trends in Food Science and Technology*, *99*(August 2019), 58–75. https://doi.org/10.1016/j.tifs.2020.02.021

Stanyon, H. F., Cong, X., Chen, Y., Shahidullah, N., Rossetti, G., Dreyer, J., Papamokos, G., Carloni, P., & Viles, J. H. (2014). *Developing predictive rules for coordination geometry from visible circular dichroism of copper (II) and nickel (II) ions in histidine and amide main-chain complexes*. *281*(Ii), 3945–3954. https://doi.org/10.1111/febs.12934

Wang, B., Timilsena, Y. P., Blanch, E., & Adhikari, B. (2017a). Characteristics of bovine lactoferrin powders produced through spray and freeze drying processes. *International Journal of Biological Macromolecules*, *95*, 985–994. https://doi.org/10.1016/j.ijbiomac.2016.10.087

Wang, B., Timilsena, Y. P., Blanch, E., & Adhikari, B. (2017b). Drying and denaturation characteristics of three forms of bovine lactoferrin. *Drying Technology*, *35*(5), 606–615. https://doi.org/10.1080/07373937.2016.1196699

Wang, B., Timilsena, Y. P., Blanch, E., & Adhikari, B. (2019). Lactoferrin : Structure , function , denaturation and digestion. *Critical Reviews in Food Science and Nutrition*, *59*, 580–596. https://doi.org/10.1080/10408398.2017.1381583

Wang, T., Bae, M., Lee, J., & Luo, Y. (2018). Solid lipid-polymer hybrid nanoparticles prepared with natural biomaterials: A new platform for oral delivery of lipophilic bioactives. *Food Hydrocolloids*, *84*, 581–592. https://doi.org/10.1016/j.foodhyd.2018.06.041

Wang, T., Ma, X., Lei, Y., & Luo, Y. (2016). Colloids and Surfaces B : Biointerfaces Solid lipid

816 nanoparticles coated with cross-linked polymeric double layer for oral delivery of
817 curcumin. *Colloids and Surface B: Biointerfaces*, *148*, 1–11.
818 https://doi.org/http://dx.doi.org/10.1016/j.colsurfb.2016.08.047

819 Wang, T., Soyama, S., & Luo, Y. (2016). Development of a novel functional drink from all
820 natural ingredients using nanotechnology. *LWT - Food Science and Technology*.
821 https://doi.org/10.1016/j.lwt.2016.06.050

822 Wang, X. Y., Guo, H. Y., Zhang, W., Wen, P. C., Zhang, H., Guo, Z. R., & Ren, F. Z. (2013).
823 Effect of iron saturation level of lactoferrin on osteogenic activity in vitro and in vivo.
824 *Journal of Dairy Science*, *96*(1), 33–39. https://doi.org/10.3168/jds.2012-5692

825 Wardhani, D. H., Wardana, I. N., Ulya, H. N., Cahyono, H., Kumoro, A. C., & Aryanti, N.
826 (2020). The effect of spray-drying inlet conditions on iron encapsulation using hydrolysed
827 glucomannan as a matrix. *Food and Bioproducts Processing*, *123*, 72–79.
828 https://doi.org/10.1016/j.fbp.2020.05.013

829 World Health Organization. (2020). *WHO guideline on use of ferritin concentrations to assess*
830 *iron status in individul and populations*.

831 Xu, K., Zhao, Z., Guo, M., & Du, J. (2019). Conjugation between okra polysaccharide and
832 lactoferrin and its inhibition effect on thermal aggregation of lactoferrin at neutral pH. *Lwt*,
833 *107*(February), 125–131. https://doi.org/10.1016/j.lwt.2019.02.082

834 Zhang, H., Li, H., Wang, J., Sun, J., Qin, A., & Tang, B. Z. (2015). Axial chiral aggregation-
835 induced emission luminogens with aggregation-annihilated circular dichroism effect.
836 *Journal of Materials Chemistry C*, *3*(20), 5162–5166. https://doi.org/10.1039/c5tc00629e

837 Zhou, M., Khen, K., Wang, T., Hu, Q., Xue, J., & Luo, Y. (2018). Chemical crosslinking
838 improves the gastrointestinal stability and enhances nu- trient delivery potentials of egg
839 yolk LDL/polysaccharide nanogels. *Food Chemistry*, *239*, 840–847.
840 https://doi.org/10.1016/j.foodchem.2017.07.019

841

Table 1 – Particles diameter mean ± standard deviation. [a–e]. Different letters mean statistically significant differences between values ($p<0.05$)

Sample	Particles diameter (µm)
NSD60_10	1.103 ± 0.588[a]
NSD60_50	0.944 ± 0.470[b]
NSD60_100	0.925 ± 0.465[b]
NSD80_10	0.907 ± 0.453[b]
NSD80_50	0.812 ± 0.433[c]
NSD80_100	1.084 ± 0.55[a]
NSD100_10	0.677 ± 0.359[d]
NSD100_50	0.905 ± 0.516[b]
NSD100_100	1.184 ± 0.541[e]

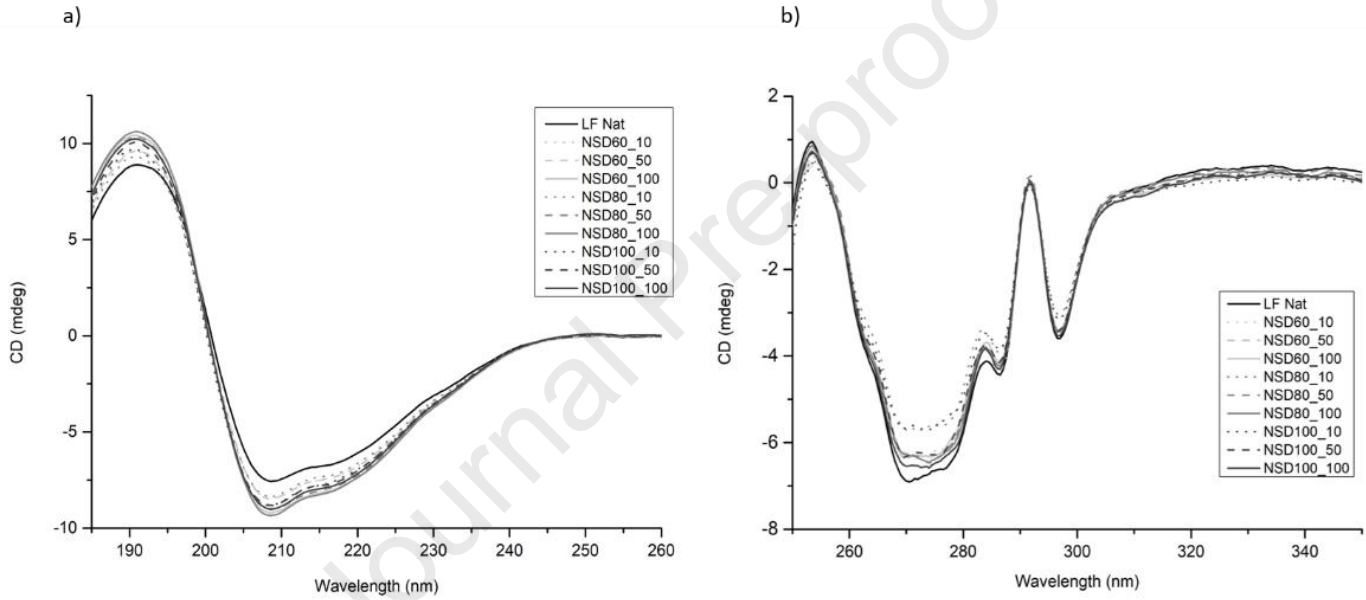

Figure 1 – a) Circular dichroism spectrum obtained for the secondary structure of the different LF concentrations and drying temperatures. b) Circular dichroism spectrum obtained for the tertiary structure of the different LF concentrations and drying temperatures.

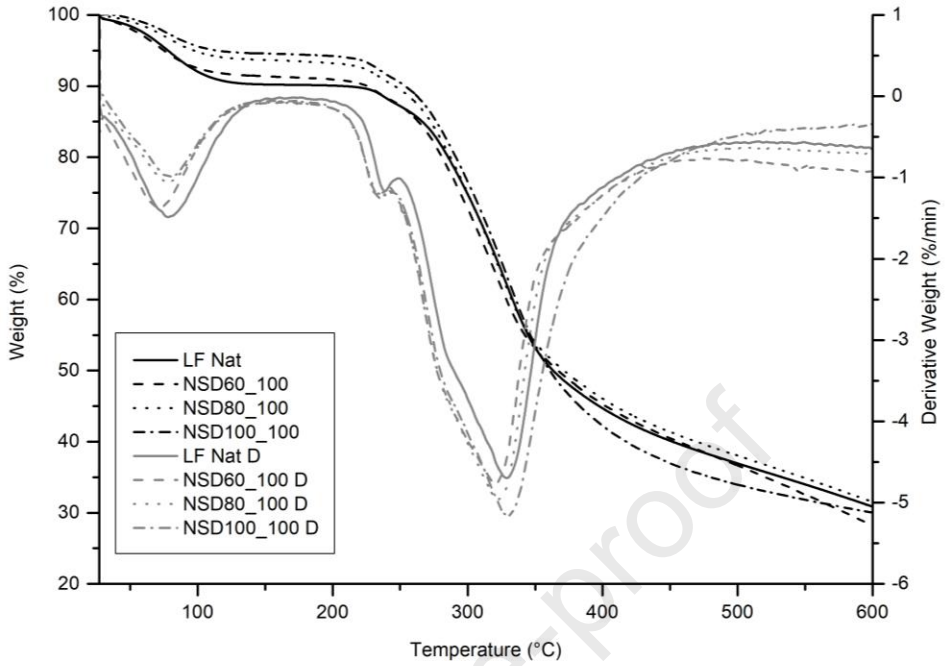

Figure 2 – Thermogravimetric analysis for LF samples after NSD at different temperatures. Derivative spectrum is identified with D in the inserted legend.

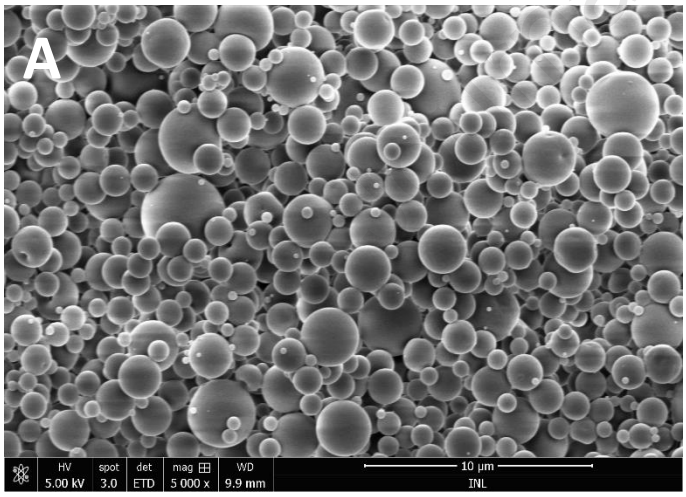

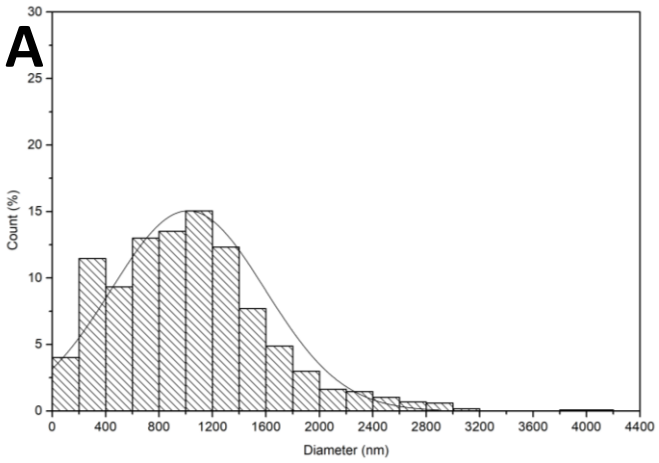

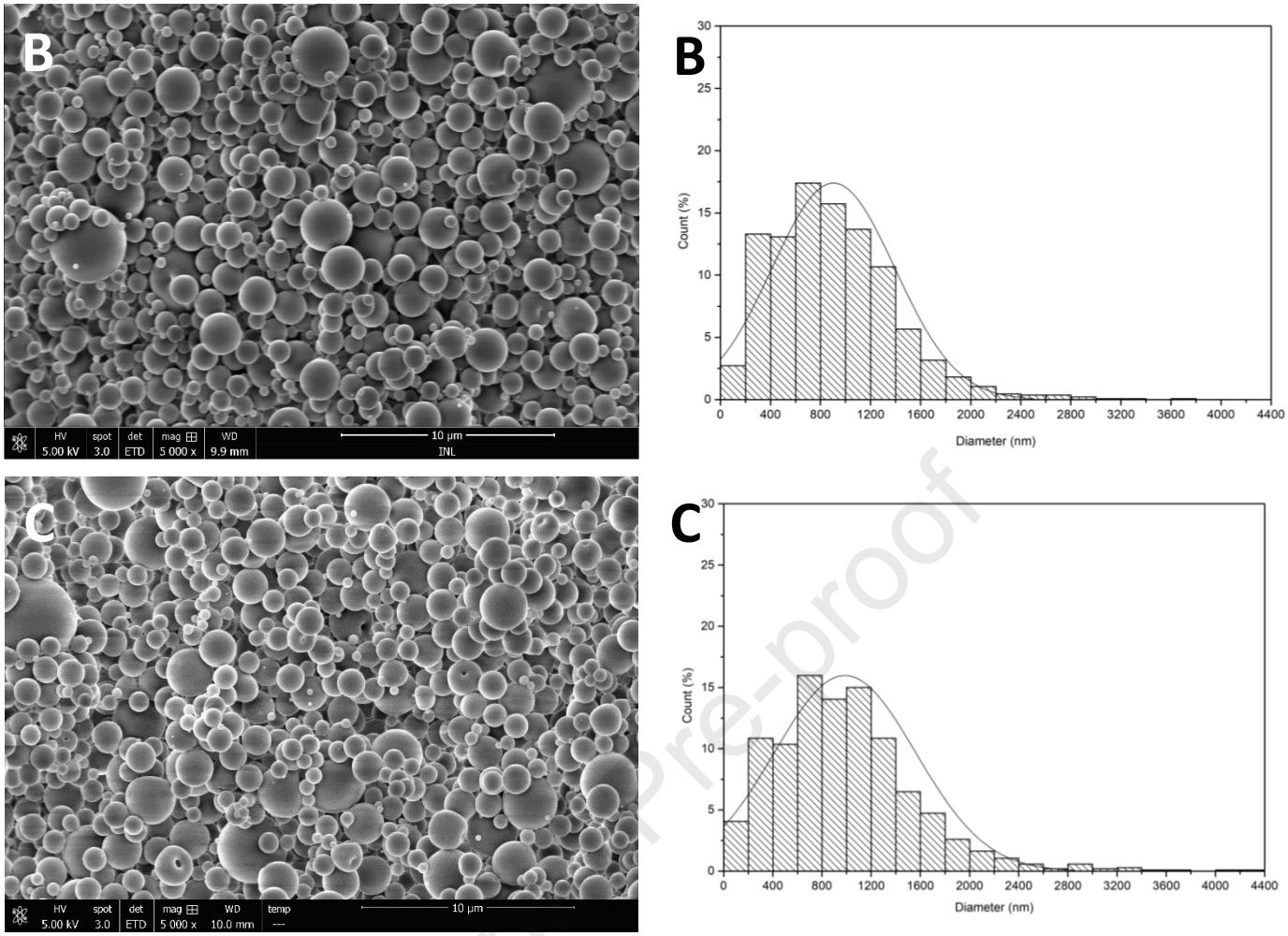

Figure 3 – SEM images and corresponding size distribution graphs: A) NSD80_100_0.7; B) NSD80_100_1.4; C) NSD80_100_2.8.

Table 2 – Particles diameter mean ± standard deviation for samples with iron addition. [a] *-* [c]*. Different letters mean statistically significant differences between values ($p<0.05$)*

Samples	Particles diameter (µm)
NSD80_100	1.084 ± 0.550 [a]
NSD80_100_0.7	1.018 ± 0.576 [a,c]
NSD80_100_1.4	0.903 ± 0.492 [b]
NSD80_100_2.8	0.987 ± 0.574 [c]

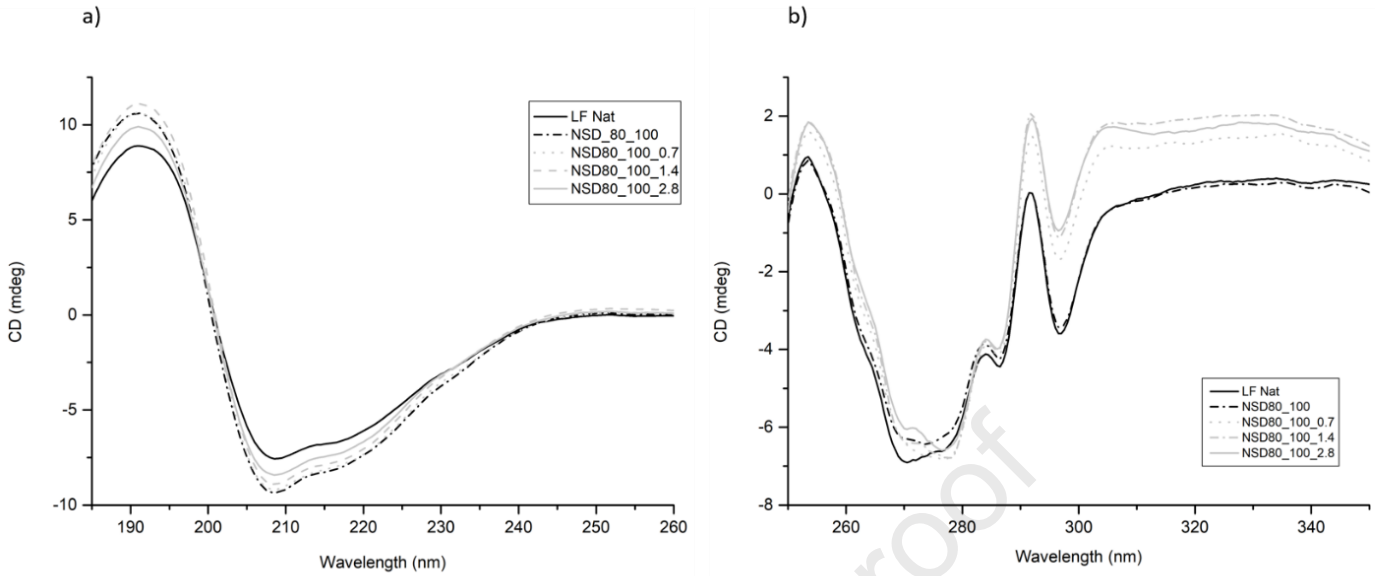

Figure 4 –Circular dichroism spectra of LF 100 mg.mL^{-1} after drying process at 80 °C with the addition of iron at different concentrations: a) Secondary structure spectra for LF Nat, NSD80_100; NSD80_100_0.7, NSD80_100_1.4, and NSD80_100_2.8; b) Tertiary structure spectra for LF Nat, NSD80_100; NSD80_100_0.7, NSD80_100_1.4, and NSD80_100_2.8.

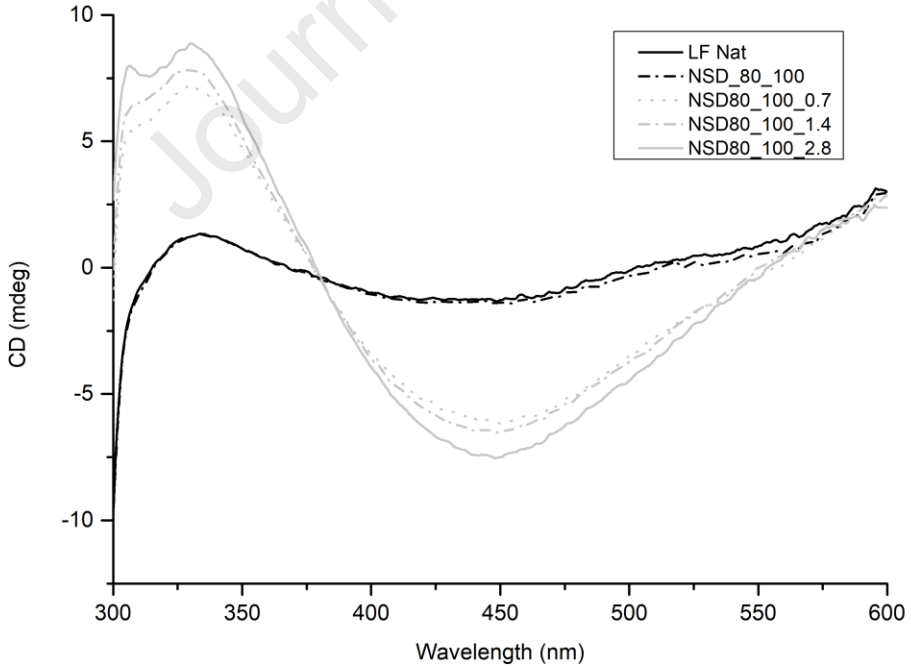

Figure 5 – Visible CD spectra (300 nm – 600 nm) to evaluate iron binding capacity to LF. NSD80_100 at different iron concentrations (0.7, 1.4 and 2.8 mg of iron per gram of LF).

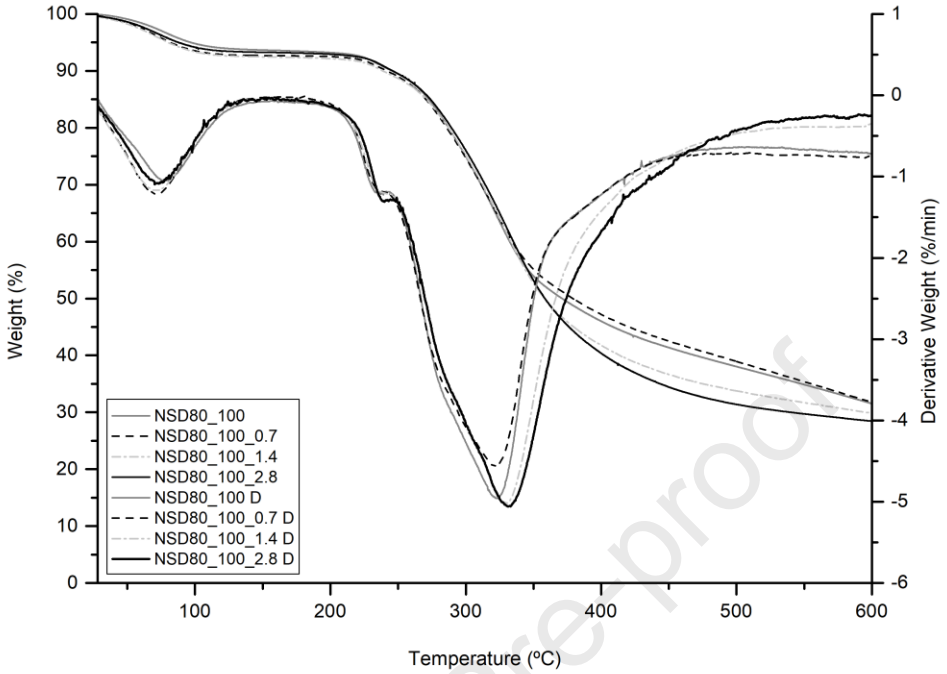

Figure 6 - Thermogravimetric analysis for NSD80_100 at different iron concentrations (0.7, 1.4 and 2.8 mg of iron per gram of LF). Derivative spectrum is identified with D in the inserted legend.

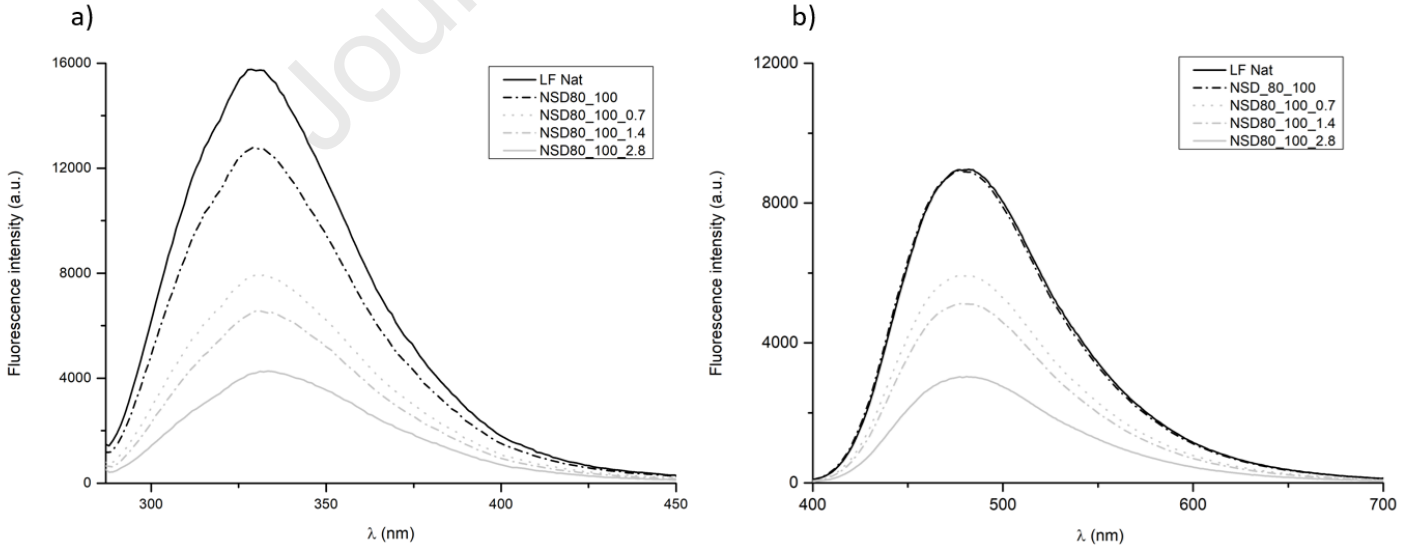

Figure 7 – a) Fluorescence emission spectra (excitation at 280 nm) of LF Nat and NSD80_100 with different iron concentrations (0.7, 1.4 and 2.8 mg of iron per gram of LF); b) ANS fluorescence emission spectra (excitation 370 nm) of LF Nat and NSD80_100 with different iron concentrations (0.7, 1.4 and 2.8 mg of iron per gram of LF).

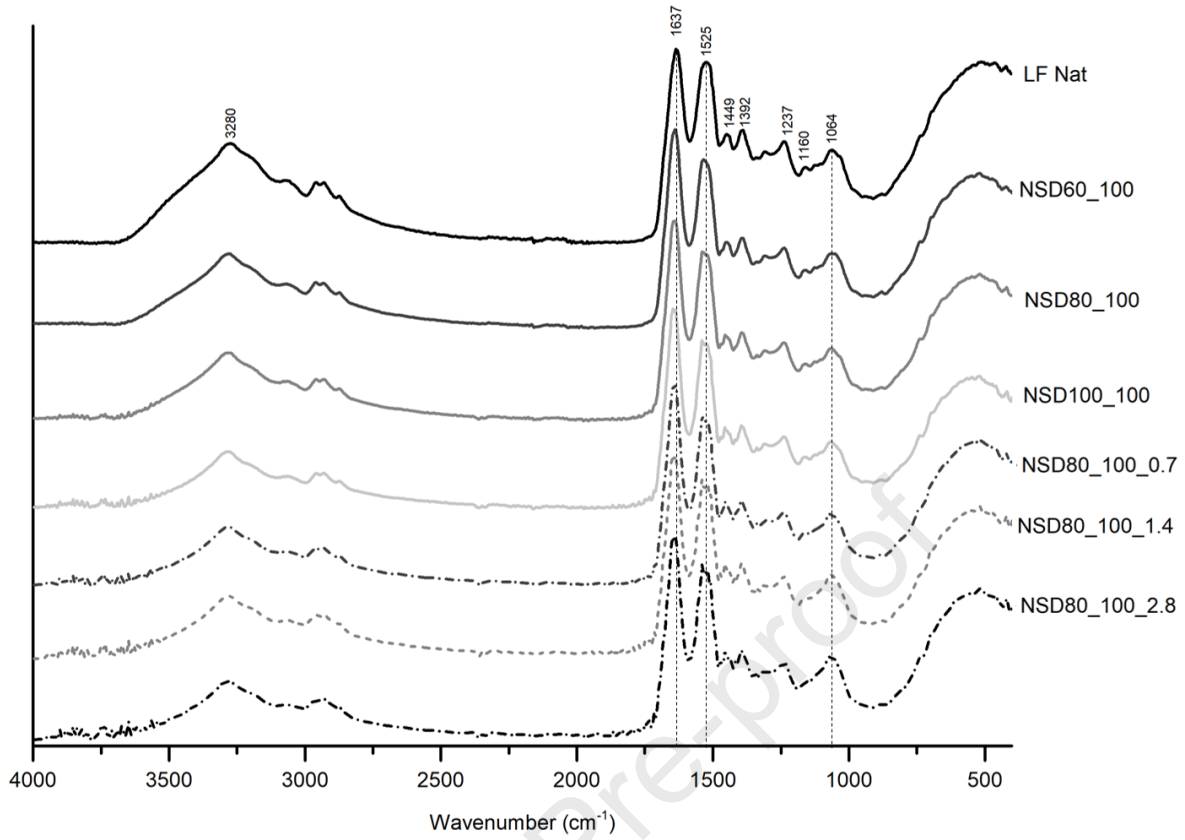

Figure 8 – FTIR spectra for LF Nat; NSD60_100 NSD80_100; NSD100_100; NSD80_10_0.7; NSD80_10_1.4; NSD80_10_2.8. Dashed vertical lines are just for orientation.

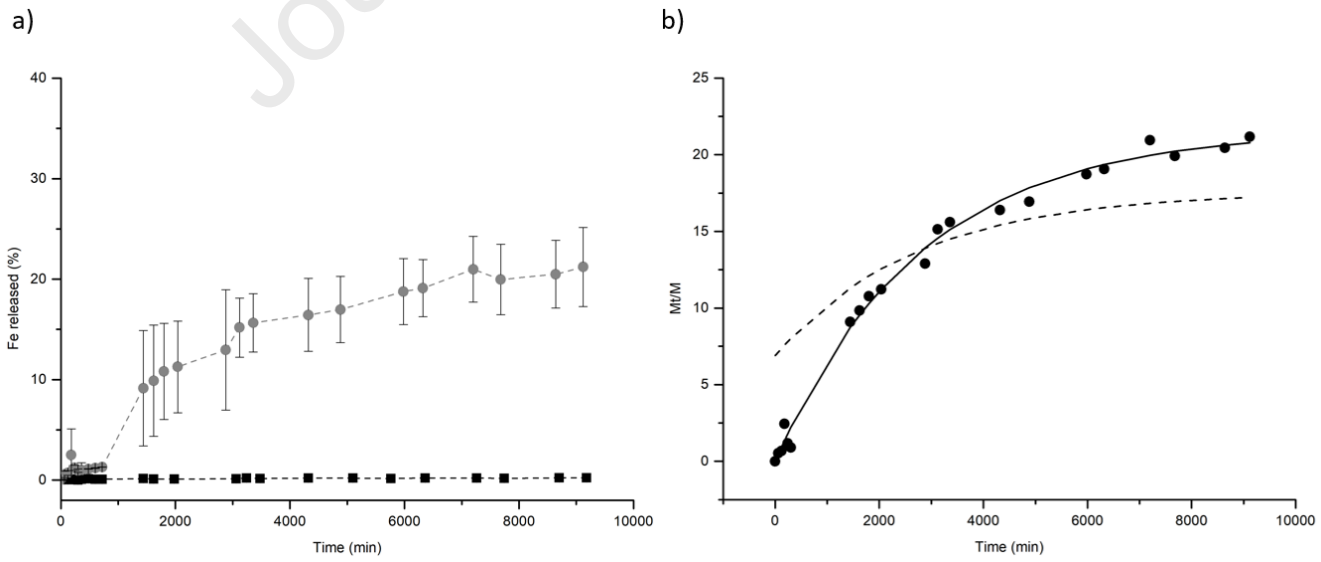

Figure 9 – a) Fe release from LF particles at pH=2 (grey) and pH=7 (black), at 37 °C. b) Iron release profile at pH 2, 37 °C. Experimental data (•); description of Fick's model (i=0) (- - -) and of Linear Superposition Model (i=1) (—).

Highlights

- Nano Spray Dryer is a suitable technology to dry protein-based carriers
- Nano Spray Dryer does not promote lactoferrin (LF) denaturation
- LF protein can be used as an iron carrier
- Iron release from LF-based carriers was pH-responsive

Declaration of interests

☒ The authors declare that they have no known competing financial interests or personal relationships that could have appeared to influence the work reported in this paper.

☐The authors declare the following financial interests/personal relationships which may be considered as potential competing interests: